

1 **Molecular dynamics simulations reveal membrane lipid interactions of the full-length** 2 **lymphocyte specific kinase Lck**

3
4
5 Dheeraj Prakaash ^{1,2}, Graham P. Cook ³, Oreste Acuto ⁴ and Antreas C. Kalli ^{1,2} *

6
7 ¹ Leeds Institute of Cardiovascular and Metabolic Medicine, School of Medicine, University of
8 Leeds, United Kingdom.

9 ² Astbury Center for Structural Molecular Biology, University of Leeds, United Kingdom.

10 ³ Leeds Institute of Medical Research, School of Medicine, University of Leeds, United Kingdom.

11 ⁴ Sir William Dunn School of Pathology, University of Oxford, United Kingdom.

12
13 * Correspondence: a.kalli@leeds.ac.uk

14
15
16 Short title: Simulations of the full-length Lck

17 18 19 **Keywords**

- 20
21 • Full-length Lck
22 • Molecular dynamics simulations
23 • Protein-lipid interactions
24 • Protein conformation

25 26 27 **ABSTRACT**

28
29 The membrane-bound lymphocyte-specific protein-tyrosine kinase (Lck) triggers T cell antigen
30 receptor signalling to initiate adaptive immune responses. Despite many structure-function studies,
31 the mode of action of Lck and the potential role of plasma membrane lipids in regulating Lck's
32 activity remains elusive. Advances in molecular dynamics simulations of membrane proteins in
33 complex lipid bilayers have opened a new perspective in gathering such information. Here, we have
34 modelled the full-length Lck open and closed conformations available from crystallographic studies
35 and simulated its interaction with the inner leaflet of the T cell plasma membrane. In both
36 conformations, we found that the unstructured unique domain and the structured domains including
37 the kinase interacted with the membrane with a preference for PIP lipids. Interestingly, our
38 simulations suggest that the Lck-SH2 domain interacts with lipids differently in the open and closed
39 Lck conformations, demonstrating that lipid interaction can potentially regulate Lck's conformation
40 and in turn modulate T cell signalling. Additionally, the Lck-SH2 and kinase domain residues that
41 significantly contacted PIP lipids are found to be conserved among the Src family of kinases,
42 thereby potentially representing similar PIP interactions within the family.

44 INTRODUCTION

45

46 Activation of T cells is triggered by the engagement of the T cell receptor (TCR) with antigenic
47 peptides presented by major histocompatibility complexes (pMHC) (Courtney, Lo, & Weiss, 2018;
48 Mariuzza, Agnihotri, & Orban, 2019). Upon pMHC binding, allosteric sites in the extracellular and
49 transmembrane regions of the T cell receptor-CD3 complex (TCR-CD3) (He et al., 2020; Lanz et
50 al., 2021) promote exposure of immunoreceptor tyrosine-based activation motifs (ITAMs) in the
51 cytoplasmic tails of CD3/ ζ subunits. Further, ITAMs are promptly phosphorylated by Lck.
52 Remarkably, non-activated T cells maintain a sizable fraction of constitutively activated Lck at the
53 plasma membrane that is necessary and sufficient for ITAM phosphorylation upon ligand binding
54 (Nika et al., 2010). Additionally, imaging studies have suggested that Lck conformational states
55 dictate its spatial distribution that may impact TCR-CD3 ITAM phosphorylation (Rossy, Owen,
56 Williamson, Yang, & Gaus, 2013). Phosphorylated ITAMs then provide stable binding sites for the
57 tyrosine kinase ZAP-70 (Hatada et al., 1995; Katz, Novotná, Blount, & Lillemeier, 2017) that is
58 regulated by Lck to propagate signals required for T cell activation (Palacios & Weiss, 2004).

59

60 Understanding the role of Lck in molecular detail is important in deciphering the initial phases of T
61 cell activation. To achieve this, it is key to obtain the full-length 3D structure of Lck which remains
62 structurally unresolved until date. The full-length Lck contains the following domains (from the *N*
63 to *C* terminus): the SH4 (first ~10 residues), unique domain (UD; following ~50 residues) both of
64 which are likely to be devoid of secondary structure. The UD is followed by the SH3, SH2, and the
65 kinase domains for which structural data is available. The X-ray crystallographic structure of the
66 Lck-SH2 and SH3 domains combined is available at a resolution of 2.36 Å (PDB:4D8K), and the
67 isolated kinase domain in its active state i.e., phosphorylated at Y394 is available at 1.7 Å resolution
68 (PDB:3LCK) (Yamaguchi & Hendrickson, 1996). However, the structures of the SH4 and UD
69 remain largely unresolved. Nonetheless, NMR data for Lck-UD in solution indicates that it lacks
70 structure and has no significant influence on Lck-SH3 (Briese & Willbold, 2003). In this work, we
71 refer to the SH4 and the UD combined as the ‘SH4-U’ domain for simplicity. In the SH4 domain,
72 G2, C3 and C5 undergo acylation as a post-translational acylation i.e., myristoylation at G2
73 (Udenwobele et al., 2017; Wingfield, 2017), and palmitoylation at C3 and C5 (Yurchak & Sefton,
74 1995). As a result, the acyl chains or lipid tails covalently attached to these residues insert into the
75 hydrophobic core of the membrane and aid in membrane localization of Lck (MD, 1994).

76

77 Lipids in the inner leaflet of the plasma membrane have been reported to play an important role in
78 interacting with Lck via its SH2 domain and in turn regulating TCR-CD3 signalling (Sheng et al.,
79 2016). In particular, anionic lipids such as phosphatidylinositol-4,5-bisphosphate (PI(4,5)P₂ or PIP₂)
80 and phosphatidylinositol-3,4,5-triphosphate (PIP₃) were suggested to aid in Lck interaction with the
81 TCR-CD3 in a spatiotemporal manner. Lck-SH2 domain is found to be key to lipid interaction by
82 selectively contacting these PIP lipids via a cationic patch (Sheng et al., 2016). SH2 domains in
83 other tyrosine kinases such as Zap70 have also been reported to direct signalling pathways by
84 binding to PIP lipids (Park et al., 2016). Our previous studies suggested that the TCR-CD3
85 maintains an anionic lipid environment enriched in PIP lipids with the help of its cytoplasmic region
86 (Prakaash, Cook, Acuto, & Kalli, 2021). Since Lck is also shown to possess high affinity for PIP
87 lipids (Sheng et al., 2016) and its clustering is driven by their open conformational state (Rossy et
88 al., 2013), it is important to understand how the open and closed states of Lck interact with the

89 membrane in molecular detail. This could further aid in our understanding of its interaction with
90 ITAMs of stimulated TCR-CD3 complexes.

91
92 In this study, we modelled the full-length Lck by predicting the structure of the SH4-U domain and
93 integrating it with the experimentally resolved structures of the SH2, SH3 and kinase domains.
94 Further, we performed coarse-grained molecular dynamics simulations over a cumulative time of
95 100 microseconds for each of the open and closed states of Lck in a complex symmetric bilayer
96 whose lipid headgroup composition resembles the inner leaflet of the T cell plasma membrane
97 (Zech et al., 2009). From these simulations, we study the conformational dynamics and lipid
98 interactions of the open and closed conformations of the full-length Lck.

99

100

101 **RESULTS and DISCUSSION**

102

103 **Modelling the full-length Lck in its open and closed states**

104 To obtain a model of the 3D structure of full-length Lck, we first modelled the SH4-U domain since
105 its structure is unknown. To achieve this, we used two independent 3D structure prediction tools
106 i.e., I-Tasser (Yang et al., 2015) and Robetta (D. E. Kim, Chivian, & Baker, 2004), and obtained
107 multiple 3D models from each. Then, the PSIPRED Protein Analysis Workbench (Buchan & Jones,
108 2019) was used to calculate the secondary structure of the SH4-U domain (**Fig S1A**). The best 3D
109 structural models, one from I-Tasser and one from Robetta (representing the highest prediction
110 confidence score and agreement with secondary structure predictions) were subjected to 250 ns
111 atomistic molecular dynamics (ATMD) simulations in solution neutralized by 0.15M Na⁺ and Cl⁻
112 ions to allow optimization of the predicted structures. At the end of the ATMD simulations, we used
113 two criteria to select the best model: (i) agreement with secondary structure predictions, and (ii)
114 agreement with structural information revealed by an NMR study (P. W. Kim, Sun, Blacklow,
115 Wagner, & Eck, 2003) where the UD contained a hairpin-like loop region (**Fig 1A left**). This loop
116 region was found to be responsible for binding CD4 and CD8 co-receptors via a coordinating Zn²⁺
117 ion (P. W. Kim et al., 2003), though data have indicated that not all Lck are bound to co-receptors.
118 Using these criteria, the model derived from the Robetta server was selected. However, due to the
119 absence of a zinc ion in our model, a disulphide bond was formed. In addition, our model suggests
120 that residues E10, D11, D12, E15, E21 (**Fig 1A**) form an anionic patch that potentially interact with
121 cationic regions of the TCR-CD3 cytoplasmic region. Moreover, the D12N mutation was shown to
122 reduce binding with CD3ε BRS by NMR experiments (Li et al., 2017).

123

124 Following modelling of the SH4-U domain, the crystal structures of SH2, SH3 (PDB:4D8K), and
125 kinase domains (PDB:3LCK) along with the SH4-U model were assembled in a linear manner to
126 model the full-length Lck open conformation (**Fig 1B**) using UCSF Chimera (Pettersen et al.,
127 2004). Missing residues located in the linker region were predicted to be unstructured and hence
128 modelled as loops between the domains using Modeller 9.2 (Webb & Sali, 2014). The structures of
129 the different domains were assembled sufficiently far from each other to avoid bias in protein-
130 protein interactions at the beginning of the simulations. Note that the positioning of the SH3 and
131 SH2 domains relative to each other were not altered and were used as obtained from the crystal
132 structure (PDB:4D8K).

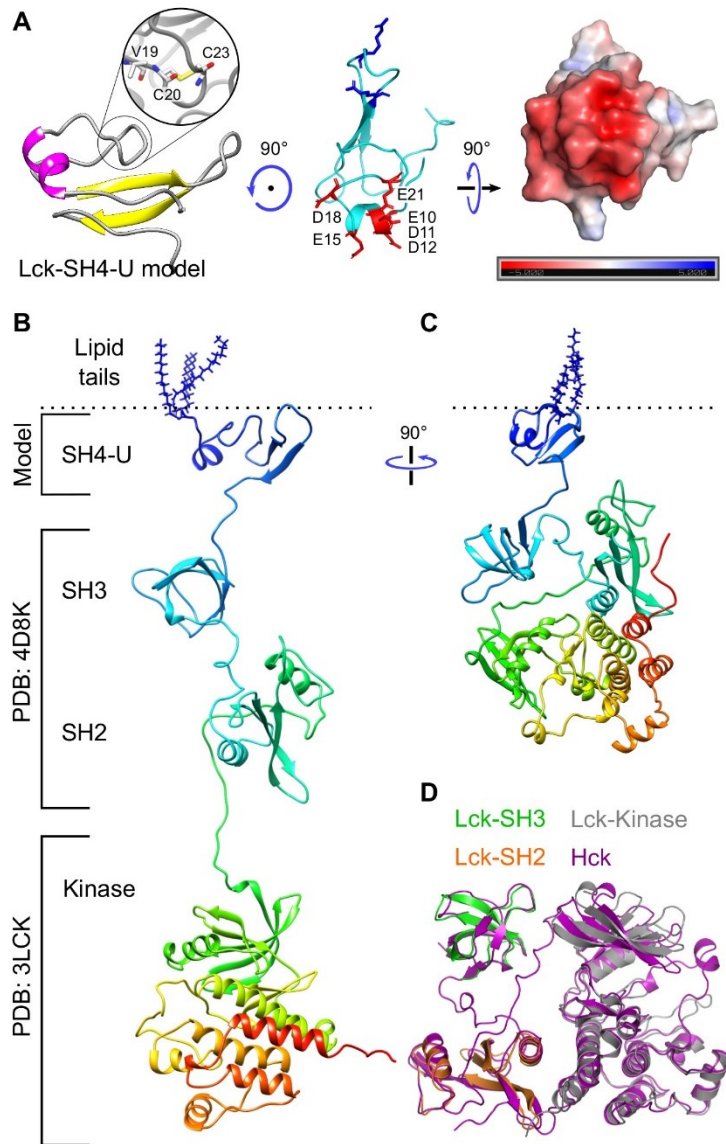
133

134 The crystal structure of the closed conformation of Hck, an Src family member of kinases, resolved
135 at 1.65 Å (PDB:5H0B) was used as a template to model the Lck closed state using Modeller 9.2
136 (Webb & Sali, 2014). The resultant homology model of the Lck closed state (containing SH2, SH3,
137 kinase domains) was then conjoined with the SH4-U model (as shown in **Fig 1A**) to obtain the full-
138 length Lck (Lck-FL) in its closed state (**Fig 1C**). This modelling used a multiple sequence
139 alignment of Hck and Lck produced by Clustal Omega (Sievers & Higgins, 2018). The structures of
140 the SH2, SH3, kinase domains of Lck were also individually aligned with those respective domains
141 of Hck (**Fig 1D**) using the ‘super’ aligning method in PyMOL (pymol.org) indicating their structural
142 similarities i.e., RMSD = 0.582, 1.135, 0.92 Å respectively.

143
144 Finally, to both the Lck-FL open and closed models, post-translational modifications were added to
145 the *N*-terminal residues i.e., G2 was myristoylated and, C3 and C5 were palmitoylated prior to the
146 simulations. The initiator Met1 residue was removed during this process since they are known to be
147 cleaved in mature eukaryotic proteins (16, 17).

148

149



150
151

152 **Fig 1. Model of the SH4-U domain and, the open and closed full-length Lck conformations.** (A)
153 The model of the SH4-U domain (residues 2 to 63) used in this study. The region responsible for
154 coordinating a Zn^{2+} ion is magnified (left). Residues forming the anionic patch in our model are
155 shown as red sticks and labelled. PIP lipid binding cationic residues (R39, R45), as suggested in
156 this study, are shown as blue sticks are located on the opposite side of the anionic patch (middle).
157 The electrostatic profile of the anionic patch (right) shown was calculated in the ± 5 kT/e range and
158 at pH 7.0 using the PDB2PQR (Dolinsky, Nielsen, McCammon, & Baker, 2004) and APBS (Baker,
159 Sept, Joseph, Holst, & McCammon, 2001) tools. Electronegative and electropositive regions are
160 indicated by red and blue intensities respectively. (B) The model of the open Lck-FL conformation
161 and (C) the closed Lck-FL conformation used in this study. (D) Isolated SH2, SH3 and kinase
162 domains aligned to the closed state of Hck (PDB:5H0B).

163

164 Membrane association and lipid interaction of the full-length Lck

165 To assess the association of the Lck-FL models with the membrane (see **Table 1** for membrane
166 composition), we performed coarse-grained molecular dynamics (CGMD) simulations. At the
167 beginning of these simulations, the post-translational modifications (lipid tails) of both the Lck-FL

168 open and closed models were made to partially penetrate the membrane surface to mimic the fact
169 that the lipid tails are expected to penetrate the membrane upon binding of Lck to the membrane. 20
170 individual simulations for 5 μ s were performed for both the open and closed models. Calculation of
171 the average distance versus time of the center of mass (COM) of the initial protein model to the
172 COM of the membrane along the vertical (Z) axis showed that both Lck-FL models closely
173 associated with the membrane within 1 μ s simulation time (**Fig 2A**). Analysis of Lck interactions
174 with lipids shows an increase in the number of PIP₂ and PIP₃ around the protein in both its open and
175 closed conformations creating an anionic annulus around the protein. This annulus was retained for
176 the remaining time of the simulations (**Fig 2B**). For both models, radial distribution function (RDF)
177 showed that PIP₂ and PIP₃ were preferred by Lck over other lipids (**Fig 2C**). Experimental studies
178 also suggest that the SH2 domain prefers to interact with PIP₃ compared to PI(4,5)P₂ (Sheng et al.,
179 2016). Interestingly, these lipid species were found to also cluster around the TCR-CD3 and interact
180 with its cytoplasmic region as observed in our previous studies of the complete TCR-CD3 complex
181 (Prakaash et al., 2021).

182
183
184

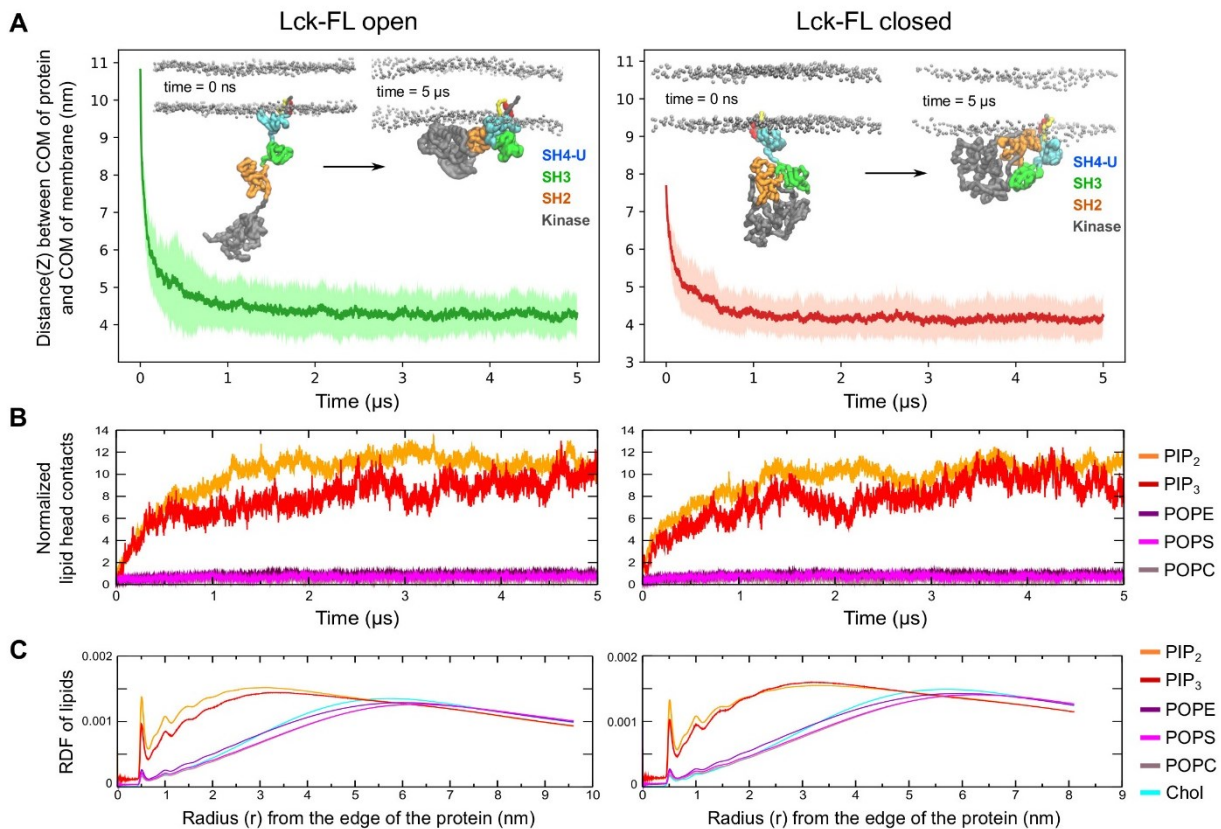
Table 1. Summary of CGMD simulations conducted in this study.

Simulations	Membrane	Particles	Simulation box (X × Y × Z axis)	Duration	Replicas
Lck-SH4-U	simple	22134	12 × 12 × 17	1 μ s	20
Lck-SH3	simple	25676	12 × 12 × 20	1 μ s	20
Lck-SH2	simple	25914	12 × 12 × 20	1 μ s	20
Lck-SH2,3,4-U	complex	53576	16 × 16 × 23	5 μ s	20
Lck-FL open	complex	83137	19 × 19 × 26	5 μ s	20
Lck-FL open mut5	complex	83194	19 × 19 × 26	5 μ s	20
Lck-FL closed	complex	46187	16 × 16 × 20	5 μ s	20

(Symmetric) membrane composition:

- simple: POPC/POPS/PIP₂/PIP₃ = 72/20/6/2
- complex: POPC/POPE/POPS/Chol/PIP₂/PIP₃ = 12/40/20/20/6/2

185
186



187

188

189

190

191

192

193

194

195

196

197

198

199

200

201

202

203

204

205

206

207

208

209

210

211

212

213

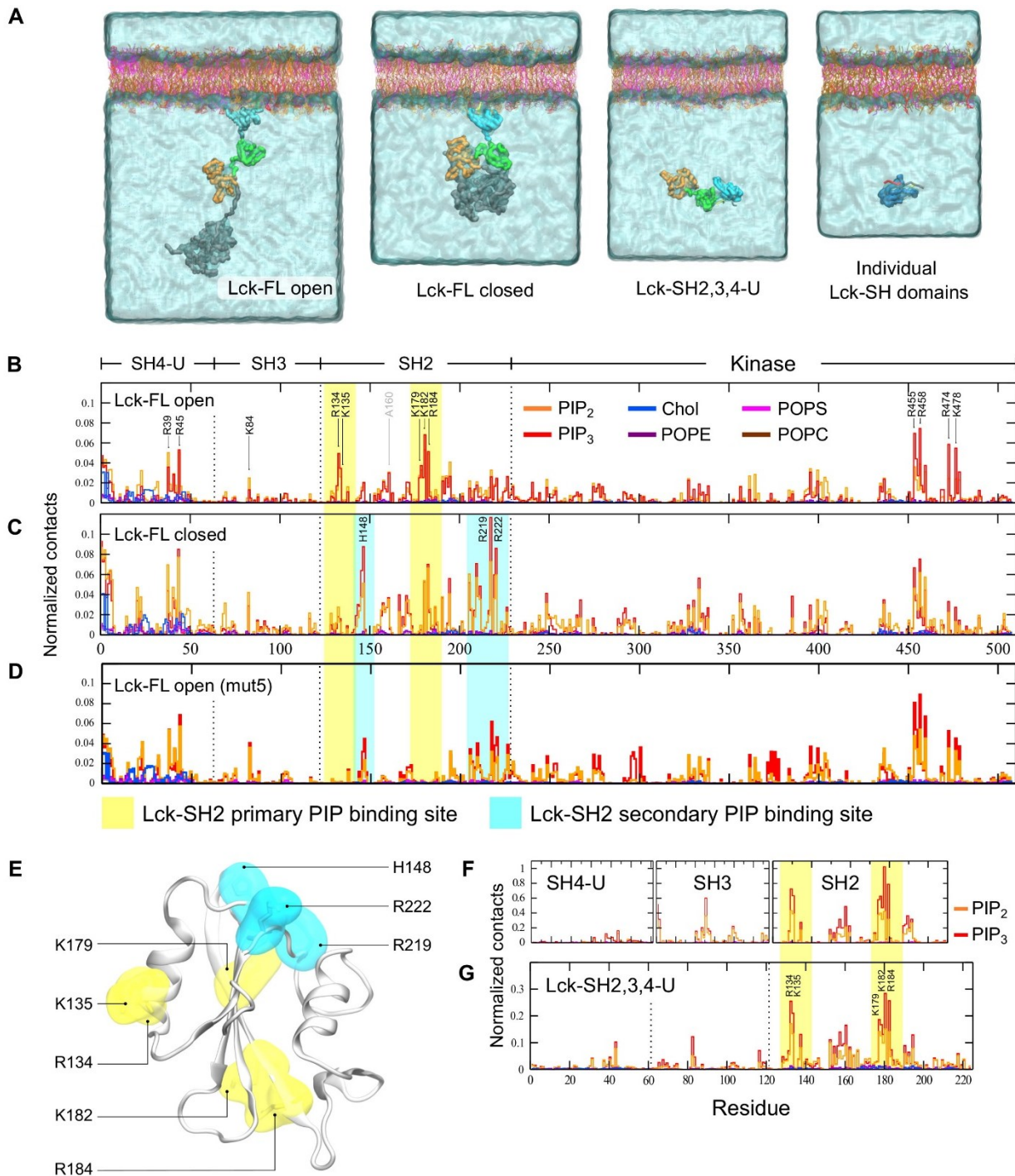
Fig 2. Membrane association and lipid interactions of the open and closed full-length Lck conformations. (A) Association of open and closed conformations of Lck-FL with the membrane is indicated by the reduction in distance between the center of mass (COM) of Lck-FL and COM of the membrane versus time. (B) Number of interactions between Lck and lipid headgroups versus time. The number of headgroup interactions of each phospholipid type is normalized by the number of lipids of the respective lipid type in the membrane. (C) The radial distribution function (RDF) of all lipid types around Lck calculated throughout the simulation time. The RDF is normalized by the total number of lipids in the membrane of that system to enable comparison between the open and closed conformations of Lck-FL. Note: Simulations of the Lck-FL open and closed systems contain different number of lipids in the membrane due to different sizes of the membrane.

Given the potential of strong electrostatic interactions between Lck and PIP lipids, and also between the TCR-CD3 cytoplasmic tails and PIP lipids of the inner leaflet of the membrane (Prakaash et al., 2021), it is possible that TCR-Lck association and ITAM phosphorylation occurs proximal to the inner leaflet of the plasma membrane.

PIP lipid binding sites

Analysis of the interactions of the Lck-FL open conformation (initial simulation frame shown in **Fig 3A left**) with PIP lipids showed that the SH2 domain made significant contacts via a primary binding site (K182 > R184 ~ R134 > K135 ~ K179). The SH4-U domain also made significant contacts by preferring to bind to PIP lipids via R39 and R45, followed by cholesterol interactions via myristoylated G2, palmitoylated C3 and C5, followed by residues H24, Y25, P26, V44, R45, D46 (**Fig 3B**). The SH3 domain made less contact with the membrane, interacting mostly via K84. Interestingly, the kinase domain of Lck also showed significant PIP lipid interactions; the most interactive residues were R455, R458, R474, K478 (**Fig 3B**). These residues are situated at the

214 bottom surface of the C-terminal lobe of the kinase domain and constitute a flat cationic area acting
215 as a PIP lipid binding site (**Fig S1B**). Furthermore, in our simulations, residues including and
216 neighbouring A160 were observed to interact with lipids, but not as significantly as K182 and R184
217 (**Fig 3B**). This observation is consistent with mutation studies which revealed that A160K reduces
218 dissociation of Lck-SH2 from plasma membrane-mimetic vesicles (Sheng et al., 2016).
219



220
221

222 **Fig 3. Snapshots of the initial simulation setup and PIP lipid binding sites.** (A) The initial frames
223 of the simulations of the open and closed conformations of Lck-FL showing the lipid tails of the
224 SH4 domain partially inserted into the membrane at the beginning of simulation. Also, the initial
225 frames of the simulations of the Lck-SH domains combined (SH2, SH3, SH4-U) and of the
226 individual Lck-SH domains where the protein structure is placed in solution ~6 nm away from the
227 membrane. (B) Normalized lipid interactions of Lck-FL open, (C) Lck-FL closed, (D) Lck-FL open
228 when mutated (mut5 i.e., R134A, K135A, K179A, K182A, R184A), (E) Residues constituting the
229 primary (yellow) and secondary (cyan) PIP lipid binding sites of Lck-SH2 as observed in CGMD
230 simulations of Lck-FL open and closed. (F) Normalized lipid interactions of the SH4-U, SH3, SH2
231 domains when individually simulated, and (G) of the SH4-U, SH3, SH2 domains simulated in
232 conjunction (Lck-SH2,3,4-U).

233

234 In the simulations of the closed Lck-FL, the lipid interaction profile of the SH4-U, SH3, and kinase
235 domains remained fairly similar to the simulations of the open Lck-FL. However, in the closed Lck-
236 FL, the SH2 domain exhibited a distinct PIP lipid binding site (referred hereon as secondary PIP
237 binding site) consisting of residues H148, R219, and R222 (**Fig 3C**). Note that K182 and R184
238 present in the primary binding site interacted with PIP lipids in both open and closed Lck-FL.
239 However, in the closed Lck-FL, PIP interaction was mostly observed in the secondary binding site
240 via residues H148, R219, R222.

241

242 **Lck-SH2 adopts a secondary PIP lipid binding site upon mutation of the primary binding site**

243 To investigate the significance of the primary PIP lipid binding site of the open Lck-FL identified
244 above, we mutated its residues i.e., R134A, K135A, K179A, K182A, R184A. This mutation
245 (referred as mut5) in the open Lck-FL led to the loss of PIP interaction via the primary binding site
246 but formed contacts with PIPs via the secondary binding site (**Fig 3D**), thereby resembling the lipid
247 interaction profile of the closed Lck-FL (**Fig 3C**). The lipid interactions and orientations of the other
248 domains remained unaffected by this mutation in the SH2 domain.

249

250 The fact that the secondary binding site of Lck-SH2 (H148, R219, R222) is located on the opposite
251 side of the primary binding site (**Fig 3E**) and dominated PIP interaction in the closed Lck-FL
252 suggests that the closed conformation potentially alters the preferred/primary membrane-binding
253 orientation of Lck-SH2 to some degree. This suggests that Lck-SH2 can attain a secondary
254 membrane-bound conformation but is less preferred and potentially weaker. This secondary binding
255 site was observed frequently in the closed state of Lck. It was shown that Lck exhibits lesser
256 membrane binding if its preferred PIP lipid binding site K182/R184 is altered (Sheng et al., 2016).
257 The fact that Lck-membrane binding was reduced and not completely diminished indicates that this
258 secondary PIP lipid binding site may aid membrane association to a certain degree but reduce
259 colocalization with stimulated TCR-CD3 due to change in its orientation. During spatial re-
260 organization of Lck with TCR-CD3 upon activation (Rossy, Williamson, & Gaus, 2012), this
261 alteration of SH2 domain orientation and PIP lipid binding site may also reduce its competence with
262 the preferred open Lck conformation as previously suggested (Hilzenrat et al., 2020; Rossy et al.,
263 2013).

264

265 **Simulations of the isolated domains reveal similar interaction with PIP lipids**

266 Following our investigation of lipid interactions of the Lck-FL open and closed states, we also
267 simulated the Lck-SH2, SH3, SH4 domains individually to be able to analyse their lipid interactions
268 independently of the influence of the other domains. Given that the kinase domain is the largest
269 domain, constituting greater than half of the Lck-FL sequence, we also simulated the Lck-SH
270 domains combined (Lck-SH2,3,4-U) to assess their lipid interactions without the influence of the
271 kinase domain. In all the individual Lck-SH and SH2,3,4-U simulations, the protein structure was
272 placed ~6 nm away from the bilayer (**Fig 3A**) to allow it to explore all possible orientations in
273 solution before binding to the membrane.

274

275 These simulations suggested that R134, K135, K179, K182, R184 of Lck-SH2 were the most
276 interactive residues with PIP lipids, preferring PIP₃ over PIP₂ (**Fig 3F, 3G**) as suggested by previous
277 experimental studies (Sheng et al., 2016) and by our simulations with the Lck-FL models in this
278 study. Lck-SH2 was also found to bind to the membrane within 700 ns of simulation time in all

279 simulations (**Fig S1C**). The SH3 domain required somewhat more simulation time i.e., 1 μ s to bind
280 to the membrane. R89 of Lck-SH3 was the most interactive residue with PIP lipids in good
281 agreement with the simulations of the Lck-FL models. Lck-SH4-U made a very small number of
282 contacts when simulated individually (**Fig 3F**) due to the lack of a strong PIP lipid binding site and
283 because the myristoylated and palmitoylated lipid tails failed to insert into the membrane in the
284 majority of the simulations (**Fig S1C**). As a result, we found a significantly larger fraction of SH4-U
285 unbound to the membrane compared to the SH2 and SH3 (**Fig S1D**). Note that, in some individual
286 SH4-U simulations where its lipid tails inserted into the membrane, the SH4-U domain stayed
287 membrane-bound for the rest of the simulation time (**S1 Movie**).

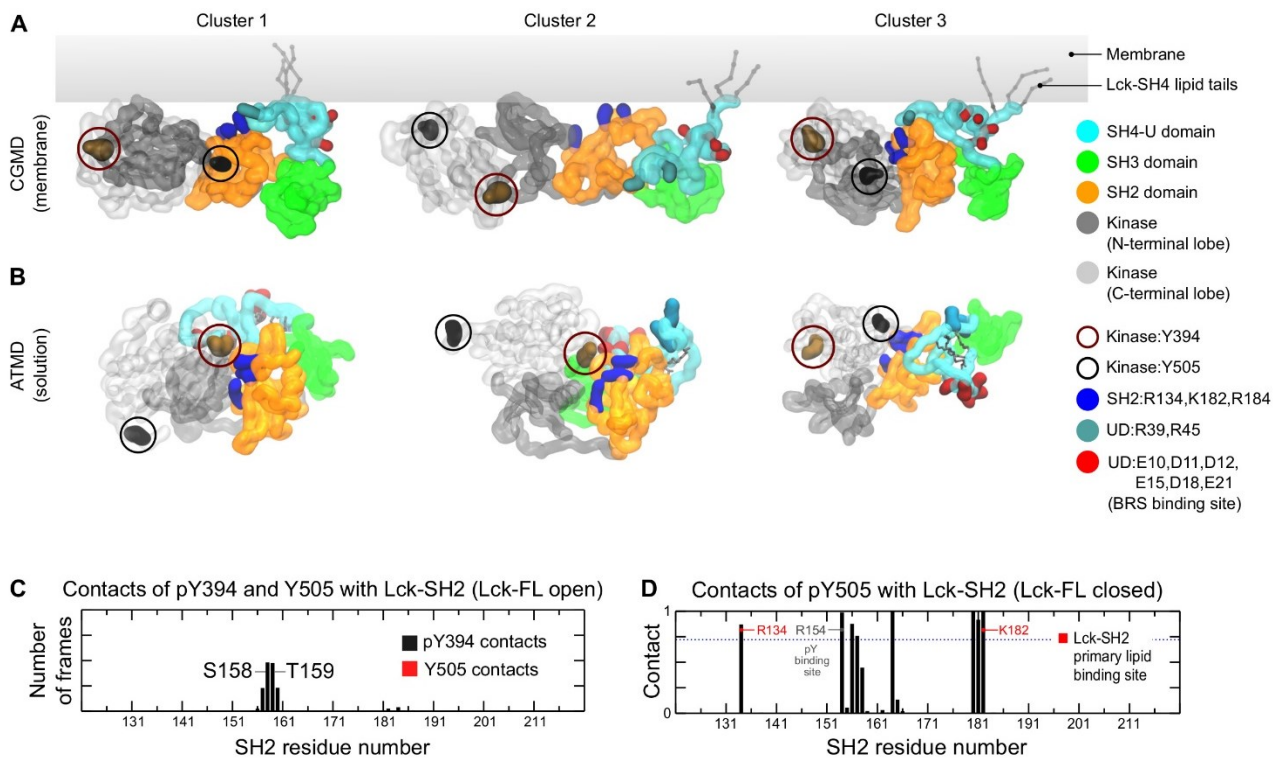
288
289 In the Lck-SH2,3,4-U simulations, the Lck-SH2 dominated the interactions with PIP lipids (with
290 R134, K135, K182, R184), while those of SH3 (K84) and SH4-U (R45) were observable but not
291 significant (**Fig 3G**). This indicated that Lck-SH2 lipid interactions were not influenced by the other
292 SH domains. Note that, although the protein had achieved a membrane bound state via the SH2
293 domain (by $\sim 1.5 \mu$ s in all simulations) (**Fig S1C bottom**), the SH4 lipid tails had not inserted in the
294 membrane. The tails were found binding to a small cavity near the SH2-SH3 linker before the
295 protein attained its membrane-bound state (**Fig S1E**) and did not insert into the membrane despite
296 lipid binding initiated by the SH2 domain. This is presumably due to strong hydrophobic
297 interactions between the lipid tails and the SH2-SH3 linker region, and possibly energetically
298 unfavourable to switch to a membrane inserted state. However, it is important to note that
299 membrane insertion may be achieved given more simulation time. Consistent with this observation,
300 *in vitro* studies have reported that the N-terminal myristoyl group in c-Src binds to the SH3 domain
301 while in solution and modulates membrane anchoring (Le Roux et al., 2019).

302 303 **Simulations of Lck-FL indicate flexibility of the kinase domain in the open conformation**

304 We deduced the most observed conformations of the membrane bound Lck-FL in its open state
305 from the CGMD simulations using clustering analysis and with a 0.35 nm RMSD cut-off. In the top
306 three most observed conformations of Lck-FL, we observed that Y394 and Y505 often switched
307 positions i.e., in one conformation, Y394 is proximal to the SH2 domain whilst in another
308 conformation, Y505 is proximal to the SH2 domain (**Fig 4A**). This indicates that the kinase domain
309 can rotate and re-orient relative to the SH2 domain. We also performed atomistic MD (ATMD)
310 simulations of the Lck-FL open state in solution (250 ns \times 3 replicas) and found similar activity of
311 the kinase domain, where pY394 and Y505 switched positions alternating their proximity to the
312 SH2 domain (**Fig 4B**).

313
314 This flexibility of the kinase domain in the Lck-FL open conformation is potentially key to the
315 dynamics of its catalytic activity. Note that, in the ATMD simulations, despite taking up positions
316 near the SH2 domain, neither pY394 nor Y505 contacted the Lck-SH2 PIP lipid binding site (**Fig**
317 **4C**) suggesting that Lck-SH2 is free to bind to the membrane in the open state, unlike in the closed
318 state where pY505 interacted with some PIP lipid binding residues of Lck-SH2 (**Fig 4D**).

319



320
321

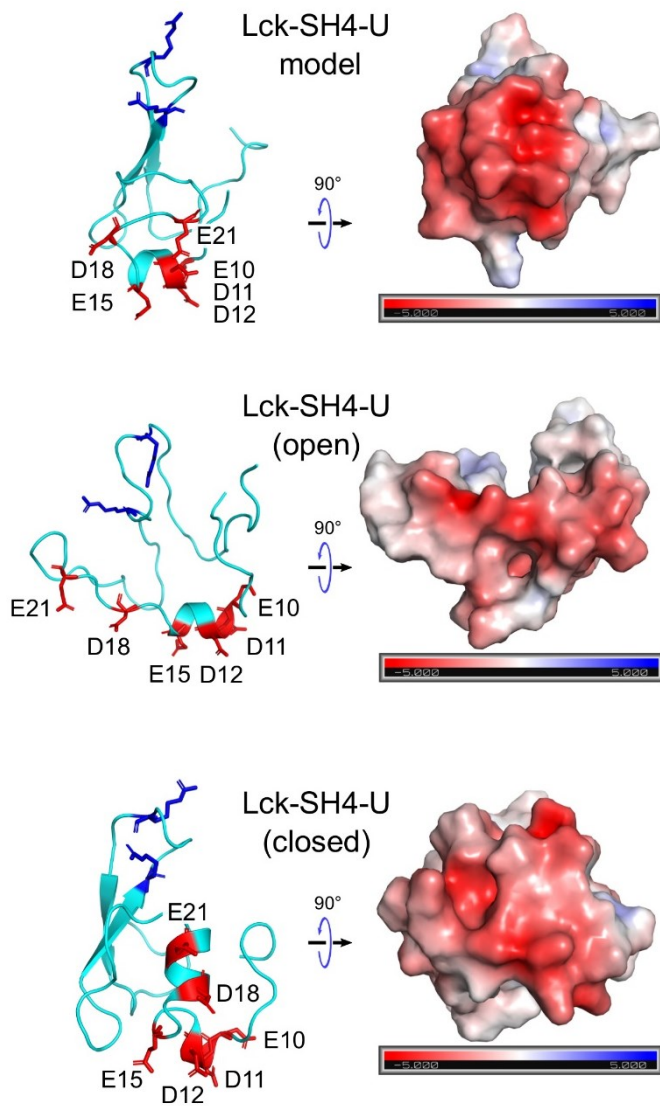
322 **Fig 4. Top three representative conformations of Lck-FL open (A) from CGMD (top) and (B)**
 323 *ATMD simulations (bottom) derived from clustering analyses (see main text for details). The kinase*
 324 *domain is made transparent to clarify the positions of Y394 and Y505. Y505 and Y394 are shown*
 325 *in circles to indicate the rotation of the kinase domain relative to the SH2 domain. This is observed by*
 326 *Y505 and Y394 exchanging positions relative to Lck-SH2, in both the membrane associated form of*
 327 *Lck (CGMD) and in solution (ATMD). (C) Normalized average number of contacts of pY394 and*
 328 *Y505 with Lck-SH2 in the open Lck-FL state. (D) Normalized average number of contacts of pY505*
 329 *with Lck-SH2 domain in the Lck-FL closed state in ATMD simulations. Normalization was done by*
 330 *dividing the number of contacts by the number of simulation frames thereby obtaining a scale of 0*
 331 *to 1.*

332

333 **Atomistic simulations of the Lck-SH4-U domain reveal its anionic patch**

334 In addition to the open Lck-FL in solution, we performed ATMD simulations of the closed Lck-FL
 335 in solution (250 ns × 3 replicas). From these simulations, clustering analyses were performed on the
 336 SH4-U domain alone. As a result, we obtained a structure of the most observed conformations of
 337 the Lck-SH4-U in the open and closed states of Lck. We then calculated their electrostatic profiles
 338 and compared them with the electrostatic profile of the initial SH4-U model obtained earlier in this
 339 study (**Fig 5**). This revealed that the SH4-U domain, despite its dynamic nature, maintained an
 340 anionic patch (E10, D11, D12, E15, D18, E21) which was independent of the open and closed Lck-
 341 FL conformations. Interestingly, this anionic patch was identified on the opposite side of its PIP
 342 lipid binding surface (R39, R45) indicating its availability to bind to cationic residues of other
 343 proteins, especially those of the BRS motifs of CD3ε and ζ subunits of the TCR-CD3 complex as
 344 suggested by NMR experiments (Li et al., 2017).

345



346
347

348 **Fig 5. The electrostatic profiles of the Lck-SH4-U domain** as in the initial model (top), and
349 according to clustering analyses after simulating the Lck-FL open state (middle), and the Lck-FL
350 closed state (bottom). Their electrostatic profiles were calculated in the ± 5 kT/e range and at pH 7.0
351 using the PDB2PQR (Dolinsky et al., 2004) and APBS (Baker et al., 2001) tools. Electronegative
352 and electropositive regions are indicated by the red and blue intensities respectively. The residues
353 forming the anionic patch are shown as red sticks and labelled. PIP lipid binding residues (R39,
354 R45) are shown as blue sticks for reference.

355
356

357 CONCLUSION

358

359 In this study, we have revealed lipid interactions of the full-length post-translationally modified Lck
360 in both its open and closed conformations and highlighted its PIP lipid binding sites. Our key
361 finding concerning PIP lipid binding was that the SH2 domain adopts a secondary binding site in
362 the closed state of Lck-FL compared to its open state. Although this secondary binding site may aid
363 in membrane localization to some degree, it may be less important during spatial organization of
364 open Lck during T cell activation. Our simulations show that upon membrane binding of Lck, it is
365 surrounded by a pool of negatively charged lipid headgroups creating an anionic environment,

366 whereas it is also observed that the TCR-CD3 cytoplasmic tails maintain an anionic lipid
367 environment (Prakaash et al., 2021). This sheds light on the potential significance of lipids during
368 TCR-Lck association.

369
370 In this study, we suggest that the residues R134, R135, and K179 contribute to the primary PIP lipid
371 binding site in addition to those previously reported i.e., K182 and R184 (Sheng et al., 2016).
372 Moreover, all five of these residues are found to be conserved among Src family members (**Fig**
373 **S2A**) indicating that all their SH2 domains are likely to localize to the membrane with the same
374 orientation. The PIP interactions of Lck-SH3, although not significant, consistently interacted via
375 K84. Upon lipid tail insertion into the membrane, the Lck-UD also showed significant interaction
376 with PIPs via R39 and R45. Furthermore, we present a structural model of the Lck-UD that reveals
377 an anionic patch with which it could bind to basic-rich motifs of the TCR-CD3 subunits and aid in
378 TCR-Lck association.

379
380 We also found that the kinase domain interacts with PIPs in the membrane via residues R455, R458,
381 R474, K478 which form a cationic patch at the bottom of its C-terminal lobe. These residues, along
382 with other potentially PIP contacting residues, were also found to be conserved among other Src
383 family members (**Fig S2A**) suggesting similar lipid interactions and membrane-bound orientations
384 of the kinase domains in the Src family. Further, the lipid interactions of the kinase domain implies
385 that it is likely to be situated proximal to the membrane surface. Therefore, given that the TCR-CD3
386 cytoplasmic region is also closely associated with the membrane surface (Prakaash et al., 2021), it is
387 likely that Lck kinase-mediated phosphorylation of TCR-CD3 ITAMs and of other downstream
388 signalling proteins during the initial phase of T cell activation is carried out proximal to the plasma
389 membrane. Similarly, given the conservation of important PIP binding sites in the SH2 and kinase
390 domains, ITAM phosphorylation mediated by other members of the Src family may also occur close
391 to the surface of plasma membrane.

392
393 It is also important to consider some limitations of this study. Here, we performed CGMD
394 simulations using the MARTINI forcefield (de Jong et al., 2013) which involved elastic network
395 (EN) restraints (Periole, Cavalli, Marrink, & Ceruso, 2009) within each domain of the open state of
396 Lck in order to maintain their tertiary structures as suggested by experiments (PDB:4D8K, 3LCK).
397 To make the open Lck simulations more realistic, we avoided inter-domain restraints allowing each
398 domain to freely associate with each other. In the closed state of Lck, it is known that the kinase
399 binds to the SH2 and SH3 domains. Therefore, such a configuration was homology modelled based
400 on the structure of the closed state of Hck, a member of the Src kinase family (PDB:5H0B) (Yuki et
401 al., 2017) found to exhibit highest identity with Lck among other Src members (**Fig S2B**). This
402 homology model of Lck was restrained using EN in CGMD simulations to retain its closed
403 conformation. The SH4-U domain was modelled based on secondary structure predictions,
404 validated using ATMD simulations and available experimental evidence, and finally conjoined with
405 the rest of the Lck structure in both open and closed conformations.

406
407

408 **METHODS**

409

410 **Molecular Modelling**

411 To obtain a model of the 3D structure of Lck-SH4-U, the PSIPRED secondary structure prediction
412 tool (Buchan & Jones, 2019) along with 3D structure predictions by the I-Tasser (Yang et al., 2015)
413 and Robetta (D. E. Kim et al., 2004) servers were used. The sequence of the SH4-U domain was
414 obtained from UniprotKB (P06239). Post-translational acylations/lipid tails were added using
415 CHARMM-GUI (Jo, Kim, Iyer, & Im, 2008). Modeller 9.2 (Eswar et al., 2006; Webb & Sali, 2014)
416 and UCSF Chimera (Pettersen et al., 2004) were used to conduct modelling of the open Lck-FL.
417 Homology modelling of the closed Lck-FL was conducted based on available structural data of Hck
418 using Modeller 9.2.

419

420 **Coarse-grained molecular dynamics (CGMD) simulations**

421 All models were coarse-grained using the Martini 2.2 forcefield (Marrink, Risselada, Yefimov,
422 Tieleman, & de Vries, 2007) and the *martinize* script. To coarse-grain the lipid tails along with the
423 rest of the protein, the *martinize* script, and the Martini 2.2 amino acid topology were modified to
424 include published parameters (Atsmon-Raz & Tieleman, 2017), and made publicly available
425 (https://github.com/DJ004/martini_mod).

426

427 CGMD simulations were set up using the *Insane* tool (Wassenaar, Ingólfsson, Böckmann, Tieleman,
428 & Marrink, 2015) and Gromacs 5.0. EN restraints (Periole et al., 2009) with a 1000 kJ/mol/nm²
429 force constant and 0 to 0.7 nm cut-off distance was applied. However, the restraints were applied
430 only within each domain to maintain their tertiary structure and not between domains to allow
431 unbiased inter-domain interactions. Membrane lipid compositions used to set up each CGMD
432 simulation are shown in Table 1. In all CGMD simulations, each lipid contained one saturated acyl
433 chain and one mono-unsaturated acyl chain, while their headgroup composition is based on the
434 composition of TCR-CD3 activation domains in the T cell plasma membrane (Zech et al., 2009).
435 The solvent was neutralized with 0.15M Na⁺ and Cl⁻ ions. All systems were energy minimized
436 using the steepest descent algorithm until the maximum force converged to 1000 kJ/mol/nm and
437 equilibrated for 2.5 ns with the protein position-restrained. The equilibrated system was then used to
438 generate differing initial velocities for twenty production simulations run for 5 μs each with a 20 fs
439 time-step. The NPT ensemble was used to conduct equilibration and production simulations. Co-
440 ordinates were saved at 200 ps intervals. A semi-isotropic Parrinello-Rahman barostat (1 bar)
441 (Parrinello & Rahman, 1981) and V-rescale thermostat (323 K) (Bussi, Donadio, & Parrinello,
442 2007) were used for production simulations along with a 3×10⁻⁴/bar compressibility.

443

444 **Atomistic molecular dynamics (ATMD) simulations**

445 CHARMM-GUI (Jo et al., 2008) was used with the CHARMM36 forcefield (Huang & MacKerell,
446 2013) to setup ATMD simulations of the initial Lck-SH4-U model, the Lck-FL open model and
447 closed model in solution using the TIP3 water as solvent neutralized with 0.15M Na⁺ and Cl⁻ ions.
448 All systems were energy minimized using the steepest descent algorithm using Gromacs 2016 until
449 the maximum force converged to 1000 kJ/mol/nm², followed by isotropic (NPT) equilibration at
450 323 K where the protein backbone was position-restrained. The equilibrated system was used to
451 generate differing initial velocities for three production simulations run 250 ns each using a 2 fs
452 time-step. Co-ordinates were saved at 40 ps intervals. The V-rescale thermostat (323 K) (Bussi et
453 al., 2007) and Parrinello-Rahman isotropic barostat (1 bar) (Parrinello & Rahman, 1981) was used

454 with a compressibility of 4.5×10^{-5} /bar. The LINCS algorithm (Hess, Bekker, Berendsen, & Fraaije,
455 1997) applied constraints on hydrogen bond lengths and the Particle Mesh Ewald algorithm
456 (Essmann et al., 1995). Coulombic and van der Waals interactions were defined by a 1.2 nm
457 distance cut-off.

458

459 **Data analysis and visualization**

460 Protein-lipid and protein-protein interactions in CGMD simulations were calculated using the *gmx*
461 *mindist* command where a contact was defined by a 0.55 nm distance cut-off. All contact analyses
462 results represent merged data from all simulation replicates. Clustering analyses used the *gmx*
463 *cluster* command and the *gromos* method (Daura et al., 1999) with an RMSD cut-off of 0.35 nm.
464 For this, all trajectories were concatenated using *gmx trjcat*, the protein was extracted using *gmx*
465 *trjconv* and RMSD calculations were run skipping 5 frames for both CGMD and ATMD. Distance
466 versus time and radial distribution function calculations were done using the *gmx distance* and *gmx*
467 *rdf* commands respectively. VMD was used for visualization and rendering (Humphrey, Dalke, &
468 Schulten, 1996). The APBS (Baker et al., 2001) plugin of PyMOL 2.4 (pymol.org) was used to
469 calculate electrostatics. Xmgrace (<https://plasma-gate.weizmann.ac.il/Grace/>) and Matplotlib 3.3
470 (doi.org/10.5281/zenodo.3948793) were used for plotting.

471

472

473 **ACKNOWLEDGMENTS**

474

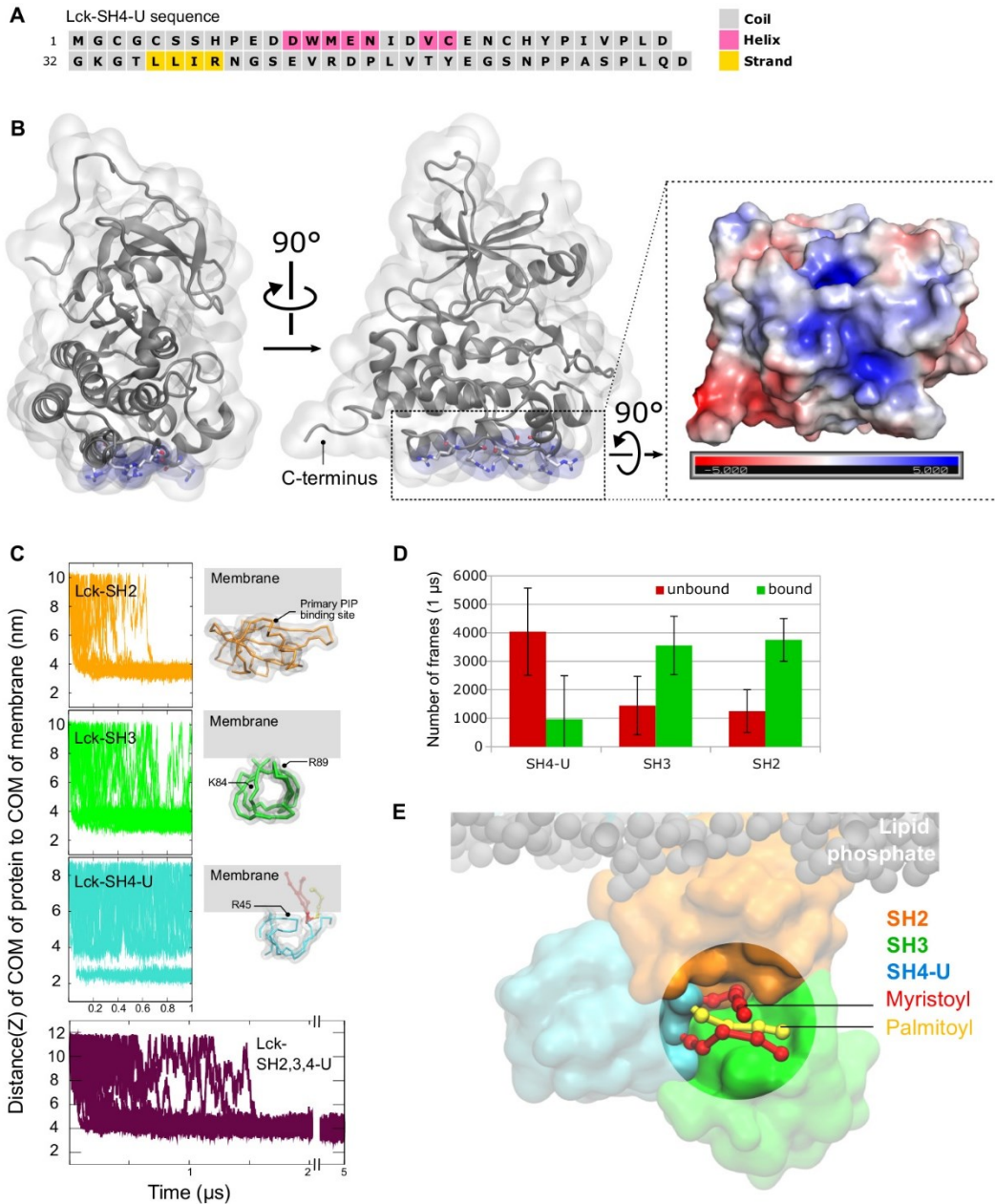
475 This research was supported by ARC3 and ARC4 supercomputers, part of the High Performance
476 Computing facility at the University of Leeds, Leeds, United Kingdom. A.C.K is funded by the
477 British Heart Foundation grant PG/21/10515. O.A. is funded by the Wellcome Trust grant
478 200844/Z/16/Z. For the purpose of open access, the author has applied a CC BY public copyright
479 licence to any Author Accepted Manuscript version arising from this submission.

480

481

482 SUPPORTING INFORMATION

483



484

485

486 **Fig S1. Secondary structure prediction of Lck-SH4-U, membrane binding of individual Lck-**
 487 **SH domains, and electrostatics of the kinase domain. (A)** Secondary structure prediction of Lck-
 488 SH4-U by PSIPRED 4.0 server. **(B)** Residues in the kinase domain forming a flat cationic patch.
 489 Their electrostatic profile was calculated using in the ± 5 kT/e range and at pH 7.0 using the
 490 PDB2PQR and APBS tools. Electronegative and electropositive regions are indicated by red and
 491 blue intensities respectively. **(C)** Distance between the center of mass (COM) of protein to COM of
 492 membrane in all 20 simulation replicates: SH4-U (cyan), SH3 (green), SH2 (orange), Lck-SH2,3,4-
 493 U (maroon). The most observed membrane-bound orientations of the individually simulated Lck-
 494 SH domains are also shown. Residues interacting most with the membrane in these simulations are
 495 labelled. **(D)** Average number of frames in the individual Lck-SH simulations that the protein stayed
 496 unbound (red) or bound (green) to the membrane. **(E)** A snapshot from one of the Lck-SH2,3,4-U
 497 simulations highlighting the binding pocket of the SH4 lipid tails (near the SH2-SH3 linker loop
 498 region) when they did not insert into the membrane.

A

CLUSTAL O(1.2.4) Multiple Sequence Alignment

```

P06241|Fyn      -----GCYQCKDKEATKLEERDGS LN--QSSGYRYGTDPTPQ 36
P12931|Src     -----GSKNSKPKDASQ---RRSLPEAENVHGAGGFAPASQ 35
P07947|Yes     -----GCISKSEKSPAIKYRPENTPEFVSTV--VSHYGAEPPTV 38
P06239|Lck     -----GC-----GCS SHPEDDW-----MENIDVCENHYPIVPLDGGK-- 32
P08631|Hck     GGRSSCEDPGCPDEERA PRMGCMKSKFLQVGG--N-TFSKTETSASPCHPVIYVDPPT-- 55
P25911|Lyn     -----GCISKRRKDLNLDDE--VDSKTQFVRNTRDTIYVRDPT-- 36
                * . . . . .
                : . . . . .

P06241|Fyn      HYPSE-----GV-TSIPNYNNFHAAGGQGLTVFVGGVNSSHTGLTRT---RGGTGVT 84
P12931|Src     -----AAEPKLFPGFNSSDVTVTSQR--AGPLAGGVT 86
P07947|Yes     SPCP---SSSAKGTAVNFSLSMT PFGSSGVT PFGGSSSVVPSY--PAGLTGGVT 93
P06239|Lck     -----GTLIRNGSEVRDPLVITYECSNPPASPLQDN 63
P08631|Hck     -----STIK--PGPNSHNSNTPGIR---EAGSEDI 80
P25911|Lyn     -----SNKQ--QRFVPEFHLLPGRFQTKDPEEQGD 65

P06241|Fyn      LFVALDYEARTEDDL SFHKGEK FQILNSEGDWWEARS LTTGETGYI PSNYVA PVD SIQ 144
P12931|Src     TFVALDYEARTEDDL SFKKEGERLQIVNTEGDWLAHSLSTGQTGYI PSNYVA PDSI Q 146
P07947|Yes     IFVALDYEARTEDDL SFKKEGERFQIINNTEGDWWEARS IATGKNGYI PSNYVA PADS I Q 153
P06239|Lck     LVIALHSYEPSHDQDLGFEKEGQLRILE-QSGEWWKASLTTQEGPI PNFVAKANSLE 122
P08631|Hck     IVVALDYEAIHHEDDL SFQGDQMVVLE-ESGEWWKARS LATRKEGYI PSNYVARVDSLE 139
P25911|Lyn     IVVALYFDGDHDDLSFKKGEKMKVLE-EHGEWWKAKS LSSKREGFI PSNYVARVNTLE 124
                : : : : :
                * * * * *
                : : : : :
                * * * * *

P06241|Fyn      AEEWYFGKLGKDAERQLLSFGNPRGTFLIRESETTKGAYSLSIRDWDMKGDHVKHYKI 204
P12931|Src     AEEWYFGKITRRESERLLLNAPNPRGTFLVRESETTKGAYCLSVSDFDNARKLVKHYKI 206
P07947|Yes     AEEWYFGMGRKDAERLLLNPNRGTFLVRESETTKGAYSLSIRDWEIRGDNVVKHYKI 213
P06239|Lck     PEPWFFKLSRDKAERQLLAPGNT HGSFLIRESETTAGS FLSVSRDFDQNGEVVKHYKI 182
P08631|Hck     TEEWFFKGISRDKAERQLLAPGNMGLSFMIRDSETTKGS YLSVSRDYDPRQGDVVKHYKI 199
P25911|Lyn     TEEWFFKIDITRDKAERQLLAPGNSAGAFIRESETLTKGS FLSVSRDYDPMHGDIKHYKI 184
                * * * * *
                : : : : :
                * * * * *
                : : : : :
                * * * * *

P06241|Fyn      RKLDNGGGYITTRAQFETLQQLVQHYSERAAAGLCCRLVVPCHGMPLRDLTSVTKDVVE 264
P12931|Src     RKLDGGGFYITSRQTFNSLQQLVAVYSKHADGLCHRLLTVCPSTKPTQGL---AKDAWE 263
P07947|Yes     RKLDNGGGYITTRAQFDTLQRLVKHYTEHADGLCHRLTVCPSTKPTQGL---AKDAWE 270
P06239|Lck     RNLNDGGFYISPRITFPGLHELVRHYTNASDGLCTRLSRCPQTKPKQKFW---WEDEWE 238
P08631|Hck     RTLNDGGFYISPRSTFTLQELVDHYKKNGLCQKLSVPCMSKPKQKFW---EKDAWE 255
P25911|Lyn     RSLDNGGYISPRITFPICSDMKHYQKSDGLCRLEKACISPKPKQKFW---DKDAWE 240
                * * * * *
                : : : : :
                * * * * *
                : : : : :
                * * * * *

P06241|Fyn      IPRESLQLIKRLGNGQGFGEVWMTNNGTTRVAIKTLKPGTMS PEFLEEAQIMKRLKHKD 324
P12931|Src     IPRESLRLEVLKQCGCFGEVWMTNNGTTRVAIKTLKPGTMS PEAFLQEAQVMKRLRHEK 323
P07947|Yes     IPRESLRLEVLKQCGCFGEVWMTNNGTTRVAIKTLKPGTMS PEAFLQEAQIMKRLKHKD 330
P06239|Lck     VPRETLKLVRELKAGQGFGEVWMTYNGHTKVAVKSLKQGSMS PDAFLAANLMKQLQHR 298
P08631|Hck     IPRESLRLEKLVKAGQGFGEVWMTYNGHTKVAVKSLKQGSMS PDAFLAANVMKTLQHDK 315
P25911|Lyn     IPRESIKLVKLVKAGQGFGEVWMTYNNSTKVAVKSLKQGSMS VQAFLEAANLMKTLQHDK 300
                : * * * * *
                : * * * * *
                : * * * * *
                : * * * * *
                : * * * * *

P06241|Fyn      LVQLYAVVS-EEPIYIVTEYMNKGSLLDFLKDGEGRALKLPNLVDMAAQVAAGMAYIERM 383
P12931|Src     LVQLYAVVS-EEPIYIVTEYMSKGSLLDFLKGEGTKYLRLPQLVDMAAQIASGMAYIERM 382
P07947|Yes     LVPLYAVVS-EEPIYIVTEYMSKGSLLDFLKGEGTKYLRLPQLVDMAAQIADGMAYIERM 389
P06239|Lck     LVRLYAVVT-QEPIYIVTEYMNKGSLLDFLKTSGIKLITINKLDMAAQIAEGMAFIEER 357
P08631|Hck     LVRLYAVVT-KEPIYIVTEYMAKGSLLDFLKSDEGSKQPLKPLIDFSAQIAEGMAFIEER 374
P25911|Lyn     LVRLYAVVTKEEPIYIVTEYMAKGSLLDFLKSDEGKVLPLKPLIDFSAQIAEGMAYIERK 360
                * * * * *
                : * * * * *
                : * * * * *
                : * * * * *
                : * * * * *

P06241|Fyn      NYIHRDLRSANI LVNGLICKIAD FGLARLIEDNEYTARQGA KFP IKWTAPEAALYGRFT 443
P12931|Src     NYVHRDLRAANI LVGENLVCKVAD FGLARLIEDNEYTARQGA KFP IKWTAPEAALYGRFT 442
P07947|Yes     NYIHRDLRAANI LVGENLVCKIAD FGLARLIEDNEYTARQGA KFP IKWTAPEAALYGRFT 449
P06239|Lck     NYIHRDLRAANI LVSDTLCKIAD FGLARLIEDNEYTAREGA KFP IKWTAPEAALYGRFT 417
P08631|Hck     NYIHRDLRAANI LVASLVCKIAD FGLARVIEDNEYTAREGA KFP IKWTAPEAALYGRFT 434
P25911|Lyn     NYIHRDLRAANLVSESLMCKIAD FGLARVIEDNEYTAREGA KFP IKWTAPEAALYGRFT 420
                * * * * *
                : * * * * *
                : * * * * *
                : * * * * *
                : * * * * *

P06241|Fyn      IKSDVWSFGILLTELVTGRVYPFGMNVREVLQVQERGYRMPCPQDCPISLHELMIHCWK 503
P12931|Src     IKSDVWSFGILLTELVTGRVYPFGMNVREVLQVQERGYRMPCPPECPESELHLMCQCWK 502
P07947|Yes     IKSDVWSFGILLTELVTGRVYPFGMNVREVLQVQERGYRMPCPQGCPESELHLMNLCWK 509
P06239|Lck     IKSDVWSFGILLTEIVTGRVYPFGMNVREVLQVQERGYRMPRPNCPPEELYQLMLRCWK 477
P08631|Hck     IKSDVWSFGILLMEIVTGRVYPFGMNVREVLQVQERGYRMPRPNCPPEELYINMRRCWK 494
P25911|Lyn     IKSDVWSFGILLVEIVTGRVYPFGMNVREVLQVQERGYRMPRPNCPDELVDIMRCWK 480
                * * * * *
                : * * * * *
                : * * * * *
                : * * * * *
                : * * * * *

P06241|Fyn      KDPEERPTFEYLQSFLEDYFTATEPOYQPGENL 536
P12931|Src     KEPEERPTFEYLQAFLEDYFTATEPOYQPGENL 535
P07947|Yes     KDPEERPTFEYLQSFLEDYFTATEPOYQPGENL 542
P06239|Lck     ERPEERPTFDYLRSLVEDYFTATEGQYQQP-- 508
P08631|Hck     NRPEERPTFEYLQSVLDDYFTATEGQYQQP-- 525
P25911|Lyn     EKAERPTFDYLRSLVEDYFTATEGQYQQP-- 511
                : : * * * * *
                : : * * * * *
                : : * * * * *
                : : * * * * *
                : : * * * * *
    
```

primary PIP binding site (SH2)

secondary PIP binding site (SH2)

significant contacts with PIPs (Kinase)

potential contact sites with PIPs (Kinase)

(Lck-PIP interactions were observed via these sites but not as significantly as those highlighted in magenta)



B

Percent Identity Matrix - created by Clustal2.1

	Fyn	Src	Yes	Lck	Hck	Lyn
P06241 Fyn	100.00	70.88	73.63	57.52	60.48	57.65
P12931 Src	70.88	100.00	75.52	54.76	58.05	54.65
P07947 Yes	73.63	75.52	100.00	56.26	62.03	57.20
P06239 Lck	57.52	54.76	56.26	100.00	66.33	63.49
P08631 Hck	60.48	58.05	62.03	66.33	100.00	72.22
P25911 Lyn	57.65	54.65	57.20	63.49	72.22	100.00

499
500
501
502
503
504
505
506

Fig S2. Multiple sequence alignment and the identity of the full-length Lck with other members of the Src family of kinases. (A) Multiple sequence alignment, obtained by Clustal Omega, highlighting the residues in the SH2 and kinase domains that mediated Lck-PIP interactions. These residues are observed to be conserved. Note that the myristoylated G2 residue is considered as the first residue, hence all residues are shifted one position behind i.e., ‘n-1’. Refer Fig 3E to visualize the primary and secondary PIP lipid binding sites of Lck-SH2. The figure shown

507 on the right is a cartoon representation of the kinase domain with significant PIP contacting residues
508 shown as magenta spheres, and potentially contacting residues shown as grey sticks. **(B)**
509 Schematic phylogenetic tree showing the evolution of Src family of kinases and their identity
510 matrix (calculated in %). This suggests that Lck is most similar to Hck compared to other Src
511 family members. The protein sequences were obtained from Uniprot (whose IDs are listed beside
512 the respective protein names).

513
514 **S1 Movie. CGMD simulation displaying insertion of myristoylated and palmitoylated lipid**
515 **tails of the SH4 domain into the membrane.** Phospholipid tails are shown as transparent grey
516 spheres and their headgroups as transparent coloured spheres (POPC: brown, POPE: purple, PIP₂:
517 orange, PIP₃: red). The myristoylated and palmitoylated residues are shown as yellow and red ball
518 and sticks respectively. Lck-SH4-U backbone is shown as white bonds, and its PIP lipid binding
519 residues R39, R45 are shown as blue surfaces.

520

521

522 REFERENCES

523

- 524 Atsmon-Raz, Y., & Tieleman, D. P. (2017). Parameterization of Palmitoylated Cysteine,
525 Farnesylated Cysteine, Geranylgeranylated Cysteine, and Myristoylated Glycine for the
526 Martini Force Field. *Journal of Physical Chemistry B*, *121*(49), 11132–11143.
527 <https://doi.org/10.1021/acs.jpcc.7b10175>
- 528 Baker, N. A., Sept, D., Joseph, S., Holst, M. J., & McCammon, J. A. (2001). Electrostatics of
529 nanosystems: Application to microtubules and the ribosome. *Proceedings of the National*
530 *Academy of Sciences of the United States of America*, *98*(18), 10037–10041.
531 <https://doi.org/10.1073/pnas.181342398>
- 532 Briese, L., & Willbold, D. (2003). Structure determination of human Lck unique and SH3 domains
533 by nuclear magnetic resonance spectroscopy. *BMC Structural Biology*, *3*(1), 1–7.
534 <https://doi.org/10.1186/1472-6807-3-3>
- 535 Buchan, D. W. A., & Jones, D. T. (2019). The PSIPRED Protein Analysis Workbench: 20 Years On.
536 *Nucleic Acids Research*, *47*(W1), W402–W407. Retrieved from
537 <https://pubmed.ncbi.nlm.nih.gov/31251384/>
- 538 Bussi, G., Donadio, D., & Parrinello, M. (2007). Canonical sampling through velocity rescaling.
539 *The Journal of Chemical Physics*, *126*(1), 014101. <https://doi.org/10.1063/1.2408420>
- 540 Courtney, A. H., Lo, W. L., & Weiss, A. (2018, February 1). TCR Signaling: Mechanisms of
541 Initiation and Propagation. *Trends in Biochemical Sciences*. Elsevier Ltd.
542 <https://doi.org/10.1016/j.tibs.2017.11.008>
- 543 Daura, X., Gademann, K., Jaun, B., Seebach, D., Van Gunsteren, W. F., & Mark, A. E. (1999).
544 Peptide folding: When simulation meets experiment. *Angewandte Chemie - International*
545 *Edition*, *38*(1–2), 236–240. [https://doi.org/10.1002/\(sici\)1521-3773\(19990115\)38:1/2<236::aid-anie236>3.0.co;2-m](https://doi.org/10.1002/(sici)1521-3773(19990115)38:1/2<236::aid-anie236>3.0.co;2-m)
- 547 de Jong, D. H., Singh, G., Bennett, W. F. D., Arnarez, C., Wassenaar, T. A., Schäfer, L. V., ...
548 Marrink, S. J. (2013). Improved Parameters for the Martini Coarse-Grained Protein Force
549 Field. *Journal of Chemical Theory and Computation*, *9*(1), 687–697.
550 <https://doi.org/10.1021/ct300646g>
- 551 Dolinsky, T. J., Nielsen, J. E., McCammon, J. A., & Baker, N. A. (2004). PDB2PQR: an automated
552 pipeline for the setup of Poisson-Boltzmann electrostatics calculations. *Nucleic Acids*
553 *Research*, *32*. <https://doi.org/10.1093/NAR/GKH381>
- 554 Essmann, U., Perera, L., Berkowitz, M. L., Darden, T., Lee, H., & Pedersen, L. G. (1995). A smooth
555 particle mesh Ewald method. *The Journal of Chemical Physics*, *103*(19), 8577–8593.
556 <https://doi.org/10.1063/1.470117>

- 557 Eswar, N., Webb, B., Marti-Renom, M. A., Madhusudhan, M. S., Eramian, D., Shen, M.-Y., ... Sali,
558 A. (2006). Comparative protein structure modeling using Modeller. *Current Protocols in*
559 *Bioinformatics, Chapter 5*, Unit-5.6. <https://doi.org/10.1002/0471250953.bi0506s15>
- 560 Hatada, M. H., Lu, X., Laird, E. R., Green, J., Morgenstern, J. P., Lou, M., ... Karas, J. L. (1995).
561 Molecular basis for interaction of the protein tyrosine kinase ZAP-70 with the T-cell receptor.
562 *Nature*, 377(6544), 32–38. <https://doi.org/10.1038/377032a0>
- 563 He, Y., Agnihotri, P., Rangarajan, S., Chen, Y., Kerzic, M. C., Ma, B., ... Orban, J. (2020). Peptide–
564 MHC Binding Reveals Conserved Allosteric Sites in MHC Class I- and Class II-Restricted T
565 Cell Receptors (TCRs). *Journal of Molecular Biology*, 432(24), 166697.
566 <https://doi.org/10.1016/j.jmb.2020.10.031>
- 567 Hess, B., Bekker, H., Berendsen, H. J. C., & Fraaije, J. G. E. M. (1997). LINCS: A linear constraint
568 solver for molecular simulations. *Journal of Computational Chemistry*, 18(12), 1463–1472.
569 [https://doi.org/10.1002/\(SICI\)1096-987X\(199709\)18:12<1463::AID-JCC4>3.0.CO;2-H](https://doi.org/10.1002/(SICI)1096-987X(199709)18:12<1463::AID-JCC4>3.0.CO;2-H)
- 570 Hilzenrat, G., Pandžić, E., Yang, Z., Nieves, D. J., Goyette, J., Rossy, J., ... Gaus, K. (2020).
571 Conformational States Control Lck Switching between Free and Confined Diffusion Modes in
572 T Cells. *Biophysical Journal*, 118(6), 1489–1501. <https://doi.org/10.1016/j.bpj.2020.01.041>
- 573 Huang, J., & MacKerell, A. D. (2013). CHARMM36 all-atom additive protein force field:
574 Validation based on comparison to NMR data. *Journal of Computational Chemistry*, 34(25),
575 2135–2145. <https://doi.org/10.1002/jcc.23354>
- 576 Humphrey, W., Dalke, A., & Schulten, K. (1996). VMD: Visual molecular dynamics. *Journal of*
577 *Molecular Graphics*, 14(1), 33–38. [https://doi.org/10.1016/0263-7855\(96\)00018-5](https://doi.org/10.1016/0263-7855(96)00018-5)
- 578 Jo, S., Kim, T., Iyer, V. G., & Im, W. (2008). CHARMM-GUI: A web-based graphical user interface
579 for CHARMM. *Journal of Computational Chemistry*, 29(11), 1859–1865.
580 <https://doi.org/10.1002/JCC.20945>
- 581 Katz, Z. B., Novotná, L., Blount, A., & Lillemeier, B. F. (2017). A cycle of Zap70 kinase activation
582 and release from the TCR amplifies and disperses antigenic stimuli. *Nature Immunology*,
583 18(1), 86–95. <https://doi.org/10.1038/ni.3631>
- 584 Kim, D. E., Chivian, D., & Baker, D. (2004). Protein structure prediction and analysis using the
585 Robetta server. *Nucleic Acids Research*, 32(Web Server issue).
586 <https://doi.org/10.1093/NAR/GKH468>
- 587 Kim, P. W., Sun, Z. Y. J., Blacklow, S. C., Wagner, G., & Eck, M. J. (2003). A zinc clasp structure
588 tethers Lck to T cell coreceptors CD4 and CD8. *Science*, 301(5640), 1725–1728.
589 <https://doi.org/10.1126/science.1085643>
- 590 Lanz, A.-L., Masi, G., Porciello, N., Cohnen, A., Cipria, D., Prakaash, D., ... Acuto, O. (2021).
591 Allosteric activation of T cell antigen receptor signaling by quaternary structure relaxation.
592 *Cell Reports*, 36(2), 109375. <https://doi.org/10.1016/J.CELREP.2021.109375>
- 593 Le Roux, A. L., Mohammad, I. L., Mateos, B., Arbesú, M., Gairí, M., Khan, F. A., ... Pons, M.
594 (2019). A Myristoyl-Binding Site in the SH3 Domain Modulates c-Src Membrane Anchoring.
595 *iScience*, 12, 194–203. <https://doi.org/10.1016/J.ISCI.2019.01.010>
- 596 Li, L., Guo, X., Shi, X., Li, C., Wu, W., Yan, C., ... Xu, C. (2017). Ionic CD3–Lck interaction
597 regulates the initiation of T-cell receptor signaling. *Proceedings of the National Academy of*
598 *Sciences of the United States of America*, 114(29), E5891–E5899.
599 <https://doi.org/10.1073/pnas.1701990114>
- 600 Mariuzza, R. A., Agnihotri, P., & Orban, J. (2019). The structural basis of T-cell receptor (TCR)
601 activation: An enduring enigma. *Journal of Biological Chemistry*. American Society for
602 Biochemistry and Molecular Biology Inc. <https://doi.org/10.1074/jbc.REV119.009411>
- 603 Marrink, S. J., Risselada, H. J., Yefimov, S., Tieleman, D. P., & de Vries, A. H. (2007). The
604 MARTINI Force Field: Coarse Grained Model for Biomolecular Simulations. *The Journal of*
605 *Physical Chemistry B*, 111(27), 7812–7824. <https://doi.org/10.1021/jp071097f>
- 606 MD, R. (1994). Myristylation and palmitoylation of Src family members: the fats of the matter. *Cell*,
607 76(3), 411–413. [https://doi.org/10.1016/0092-8674\(94\)90104-X](https://doi.org/10.1016/0092-8674(94)90104-X)
- 608 Nika, K., Soldani, C., Salek, M., Paster, W., Gray, A., Etzensperger, R., ... Acuto, O. (2010).

- 609 Constitutively active lck kinase in T cells drives antigen receptor signal transduction.
610 *Immunity*, 32(6), 766–777. <https://doi.org/10.1016/j.immuni.2010.05.011>
- 611 Palacios, E. H., & Weiss, A. (2004). Function of the Src-family kinases, Lck and Fyn, in T-cell
612 development and activation. *Oncogene*, 23(48), 7990–8000.
613 <https://doi.org/10.1038/sj.onc.1208074>
- 614 Park, M.-J., Sheng, R., Silkov, A., Jung, D.-J., Wang, Z.-G., Xin, Y., ... Cho, W. (2016). SH2
615 Domains Serve as Lipid-Binding Modules for pTyr-Signaling Proteins. *Molecular Cell*, 62(1),
616 7–20. <https://doi.org/10.1016/j.molcel.2016.01.027>
- 617 Parrinello, M., & Rahman, A. (1981). Polymorphic transitions in single crystals: A new molecular
618 dynamics method. *Journal of Applied Physics*, 52(12), 7182–7190.
619 <https://doi.org/10.1063/1.328693>
- 620 Periolo, X., Cavalli, M., Marrink, S.-J., & Ceruso, M. A. (2009). Combining an Elastic Network
621 With a Coarse-Grained Molecular Force Field: Structure, Dynamics, and Intermolecular
622 Recognition. *Journal of Chemical Theory and Computation*, 5(9), 2531–2543.
623 <https://doi.org/10.1021/ct9002114>
- 624 Pettersen, E. F., Goddard, T. D., Huang, C. C., Couch, G. S., Greenblatt, D. M., Meng, E. C., &
625 Ferrin, T. E. (2004). UCSF Chimera--a visualization system for exploratory research and
626 analysis. *Journal of Computational Chemistry*, 25(13), 1605–1612.
627 <https://doi.org/10.1002/jcc.20084>
- 628 Prakaash, D., Cook, G. P., Acuto, O., & Kalli, A. C. (2021). Multi-scale simulations of the T cell
629 receptor reveal its lipid interactions, dynamics and the arrangement of its cytoplasmic region.
630 *PLOS Computational Biology*, 17(7), e1009232.
631 <https://doi.org/10.1371/JOURNAL.PCBI.1009232>
- 632 Rossy, J., Owen, D. M., Williamson, D. J., Yang, Z., & Gaus, K. (2013). Conformational states of
633 the kinase Lck regulate clustering in early T cell signaling. *Nature Immunology*, 14(1), 82–89.
634 <https://doi.org/10.1038/ni.2488>
- 635 Rossy, J., Williamson, D. J., & Gaus, K. (2012). How does the kinase Lck phosphorylate the T cell
636 receptor? Spatial organization as a regulatory mechanism. *Frontiers in Immunology*.
637 <https://doi.org/10.3389/fimmu.2012.00167>
- 638 Sheng, R., Jung, D. J., Silkov, A., Kim, H., Singaram, I., Wang, Z. G., ... Cho, W. (2016). Lipids
639 regulate Lck protein activity through their interactions with the Lck Src homology 2 domain.
640 *The Journal of Biological Chemistry*, 291(34), 17639–17650.
641 <https://doi.org/10.1074/jbc.M116.720284>
- 642 Sievers, F., & Higgins, D. G. (2018). Clustal Omega for making accurate alignments of many
643 protein sequences. *Protein Science : A Publication of the Protein Society*, 27(1), 135–145.
644 <https://doi.org/10.1002/PRO.3290>
- 645 Udenwobe, D. I., Su, R. C., Good, S. V., Ball, T. B., Shrivastav, S. V., & Shrivastav, A. (2017,
646 June 30). Myristoylation: An important protein modification in the immune response. *Frontiers*
647 *in Immunology*. Frontiers Media S.A. <https://doi.org/10.3389/fimmu.2017.00751>
- 648 Wassenaar, T. A., Ingólfsson, H. I., Böckmann, R. A., Tieleman, D. P., & Marrink, S. J. (2015).
649 Computational lipidomics with insane: A versatile tool for generating custom membranes for
650 molecular simulations. *Journal of Chemical Theory and Computation*, 11(5), 2144–2155.
651 <https://doi.org/10.1021/acs.jctc.5b00209>
- 652 Webb, B., & Sali, A. (2014). Protein structure modeling with MODELLER. *Methods in Molecular*
653 *Biology*, 1137. https://doi.org/10.1007/978-1-4939-0366-5_1
- 654 Wingfield, P. (2017). N-Terminal Methionine Processing. *Current Protocols in Protein Science*, 88,
655 6.14.1. <https://doi.org/10.1002/CPPS.29>
- 656 Yamaguchi, H., & Hendrickson, W. A. (1996). Structural basis for activation of human lymphocyte
657 kinase Lck upon tyrosine phosphorylation. *Nature*, 384(6608), 484.
658 <https://doi.org/10.1038/384484a0>
- 659 Yang, J., Yan, R., Roy, A., Xu, D., Poisson, J., & Zhang, Y. (2015). The I-TASSER Suite: protein
660 structure and function prediction. *Nature Methods*, 12(1), 7–8.

- 661 <https://doi.org/10.1038/NMETH.3213>
- 662 Yuki, H., Kikuzato, K., Koda, Y., Mikuni, J., Yuri, T., Kukimoto-Niino, M., ... Honma, T. (2017).
663 Activity cliff for 7-substituted pyrrolo-pyrimidine inhibitors of HCK explained in terms of
664 predicted basicity of the amine nitrogen. *Bioorganic & Medicinal Chemistry*, 25(16), 4259–
665 4264. <https://doi.org/10.1016/J.BMC.2017.05.053>
- 666 Yurchak, L. K., & Sefton, B. M. (1995). Palmitoylation of either Cys-3 or Cys-5 is required for the
667 biological activity of the Lck tyrosine protein kinase. *Molecular and Cellular Biology*, 15(12),
668 6914–6922. <https://doi.org/10.1128/MCB.15.12.6914>
- 669 Zech, T., Ejsing, C. S., Gaus, K., Wet, B. de, Shevchenko, A., Simons, K., & Harder, T. (2009).
670 Accumulation of raft lipids in T-cell plasma membrane domains engaged in TCR signalling.
671 *The EMBO Journal*, 28(5), 466. <https://doi.org/10.1038/EMBOJ.2009.6>
672